EUROPEAN ORGANIZATION FOR NUCLEAR RESEARCH

CERN-SPSLC/91-21
SPSC/P261
11 March 1991

PROPOSAL

SEARCH FOR THE OSCILLATION $\nu_\mu \rightarrow \nu_\tau$

P. Astier[6], M. Banner[3], S.A. Baranov[4], Yu.A. Batusov[4], S.A. Bunyatov[4], L. Camilleri[2], R. Cormack[1], L. Dilella[2], J. Dumarchez[6], E.T. Kearns[1], O.L. Klinov[4], O.M. Kuznetsov[4], A. Letessier[6], J.M. Lévy[6], V.V. Lyukov[4], J.P. Mendiburu[5], S. Merritt[1], J.P. Meyer[3], P. Nedelec[5], Yu.A. Nefedov[4], V.I. Snyatkov[4], J.L. Stone[1], A.M. Touchard[6], F. Vannucci[6], H. Zaccone[3] and Y. Zolnierowski.

Abstract

The oscillation mode $\nu_\mu \rightarrow \nu_\tau$ may be the favoured channel to probe an effect of massive neutrinos. An experiment searching for a ν_τ signal in the CERN wide-band beam is proposed. It efficiently selects ν_τ charged current interactions by observing the τ through its electronic decay and by using kinematical criteria only. This method is complementary to the one trying to observe the creation and subsequent decay of a τ by looking for a short track. The detector is based on classical techniques. The target is made of polypropylene foils which act as a transition radiation medium and is located inside the UA1 magnet. The expected result improves the existing limits on neutrino mixings by more than one order of magnitude. Because of its excellent electron identification, the detector can accurately measure charm production. Furthermore, it is ideal to look for low energy isolated electrons or photons. This allows an investigation of some electromagnetic properties of the neutrinos.

1) Boston University, Boston, Mass, USA
2) CERN, Geneva, Switzerland
3) DPhPE, SACLAY, Gif-sur-Yvette, France
4) JINR, DUBNA, USSR
5) actual address : LPC, Collège de France, Paris, France
6) LPNHE, Univ. de Paris VI et VII, Paris, France

Due to the limited time given to write this proposal, the final decision on several detector components is not made. Different options are still being considered.

1. INTRODUCTION

As shown by e^+e^- experiments at the Z^0 peak, only three light neutrinos exist. The first two have been well studied, but the ν_τ has escaped detection so far. Several techniques are being developed to see its interactions with matter through the charged current process:

$$\nu_\tau + N \rightarrow \tau^- + X$$

This requires a very high spatial resolution detector able to recognize the very short track (typically $\sim$ 1 mm) or to reconstruct impact parameters of $\sim$ 100 μm, as expected from τ decays. We propose a complementary approach based on kinematical cuts to extract a ν_τ signal in a predominantly ν_μ beam.

The detection of the ν_τ gives a unique way to probe the possibility of neutrino mixings and non-zero masses, by looking for the oscillation $\nu_\mu \rightarrow \nu_\tau$. No firm prediction exists, but this channel may prove to be the favoured one, since it is likely that ν_τ has the largest mass among the three neutrino species. In particular, when interpreting the missing mass of the Universe as being composed of massive ν_τ, the suggested mass for the ν_τ is of the order of a few 10 eV (1). This gives rise to oscillations which could appear at the level tested in the present search if the corresponding mixing is not much smaller than the mixing angles in the quark sector.

Recent claims have been presented for the existence of a 17 keV neutrino state mixing with ν_e at a level of $|U_{e\tau}|^2 \sim 1\%$ (2). Such a heavy neutrino, if it can be identified with the third mass eigenstate, should appear in the oscillation $\nu_e \rightarrow \nu_\tau$, but also in the oscillation $\nu_\mu \rightarrow \nu_\tau$ for which the mixing $|U_{\mu\tau}|^2$ has no reason to be much smaller than $|U_{e\tau}|^2$.

2. PRINCIPLE OF THE SEARCH

2.1 Neutrino oscillations

The probability of oscillations between 2 neutrino flavours is given by:

$$P = \sin^2\,\theta\,\sin^2(\pi R/L)$$

where R is the distance between production and observation, θ is the mixing angle between the 2 neutrinos and L is the oscillation length given by:

$$L = 2.5E\ (\mathrm{GeV})/\delta m^2(\mathrm{eV}^2)\ \ (\mathrm{km})$$

with E the energy of the neutrino and $\delta m^2 = m_1^2 - m_2^2$, m_1 and m_2 referring to the neutrino mass eigenstates. The phenomenon depends on two parameters: $\sin^2 2\,\theta$ and δm^2. Limits on δm^2 vary like E/R, while limits on $\sin^2 2\,\theta$ depend on the accumulated statistics. Here we are interested in large neutrino masses (δm^2 of at least a few 100 eV^2). So the experiment can be located at a reasonable distance from the production target (of the order of 1 km). The challenge is to be sensitive to mixings as small as 10^{-4}. This region of parameters is only tested efficiently by the appearance search. To make it possible, it is compulsory to be sensitive to the presence of a few ν_τ in the predominantly ν_μ beam. Thus, the experiment requires an efficient selection of the reaction:

$$\nu_\tau + N \rightarrow \tau^- + X$$

The threshold for charged current (CC) interactions of the ν_τ is around 5 GeV. The CERN neutrino beam is perfectly adapted to this search. At SPS energies the τ track length is about 1 mm before it decays. To see the τ track, the target must have a very good spatial resolution over its whole fiducial volume. Emulsions offer such a possibility. They give the best experimental limit obtained so far (3) and proposals exist to continue with this technique, at CERN by the Charm2 collaboration and at Fermilab (4). We describe here a complementary method which only relies on kinematical criteria.

2.2 Characteristics of ν_τ events

Apart from a secondary vertex, CC ν_τ interactions differ from CC ν_μ events by the large missing p_T due to escaping neutrino(s) in τ decays. As an example, if one chooses events with a muon, they come from the reactions:

$$\nu_\mu + N \rightarrow \mu^- + X$$

and

$$\nu_\tau + N \rightarrow \tau^- + X$$

followed by $\tau^- \rightarrow \mu^- + \nu + \bar{\nu}$. The second process differs from the first one by a missing p_t of order 1 GeV/c which points near the direction of the muon transverse momentum.

The method of using kinematics to extract a ν_τ signal was advocated long ago (5), but past neutrino detectors never had the required resolution.

Instead of detecting ν_τ events through the muon decay of the produced τ, it is advantageous to consider the electron decay. The reason is that in the latter case the background is due to the charged current interactions of the ν_e component of the beam. This amounts to about 1% of the ν_μ component.

Whereas an electron trigger decreases by two orders of magnitude the ν_τ search background, it does require a target which efficiently recognizes and reconstructs genuine electrons.

3. EXPERIMENTAL SET-UP

3.1 The CERN wide-band neutrino beam

We assume 450 GeV protons for the primary beam, and a detector positioned at 940 m from the production target. This distance corresponds to the old BEBC hall. The size of the hall is such that it can accomodate the present apparatus together with the one proposed by the Charm collaboration (4). The ground can support the weight, it was reinforced for the assembly of a LEP detector.

The flux hitting the detector is computed by the standard wide band beam program. We adopt the result already calculated in (4). The energy spectrum for both ν_μ and ν_e are presented in Fig. 1. The beam contamination from direct production of ν_τ is negligibly small.

3.2 The detector

As explained above, it is necessary to reconstruct as well as possible the full kinematics of the event. This requires a magnetic spectrometer. To this purpose, we propose to use the UA1 magnet, which provides a maximum dipole field B=0.7 T in the horizontal

direction perpendicular to the beam axis over a volume 7.15 m long, 3.58 m wide and 3.34 m high. There is no problem to transport the UA1 magnet to the West Area because it can be easily disassembled into many lighter pieces.

3.2.1 Target and event rate

In order to measure charged particle momenta and to provide electron identification, we propose to install in the UA1 magnet a low density, low Z target which acts at the same time as a transition radiator. The best choice of target material would be lithium foils; however, for practical reasons polypropylene, $(C_3H_6)_n$, is an acceptable alternative.

The target is subdivided into 20 sections, each 30 cm thick and consisting of a radiator, a transition radiation detector (TRD) and a drift chamber to reconstruct charged particle tracks and measure their momenta (see Fig. 3 for a section and Fig. 2 for the overall view). Each radiator consists of 520 19 μm thick polypropylene foils spaced by 400 μm. Such a configuration has an effective density of 0.047 g/cm^3, a radiation length (r.l.) of 10.6 m and an interaction length of 18.7 m. The total mass of polypropylene contained in a fiducial volume of 2.6*2.6*5.5 m^3 amounts to 1238 kg. In such a mass an exposure of 2.4×10^{19} protons on target would provide $\sim 7.7 \times 10^5$ CC ν_μ interactions at an average neutrino energy of 48 GeV.

3.2.2 Transition radiation detectors (TRD)

The design of the transition radiator is based on a computer program which calculates the electron identification efficiency and the rejection against charged pions for a given configuration of radiator and X-ray detector. The results of the program were checked against data from UA6 and NA31(6). The information from four successive radiators having the parameters given above provides an electron identification efficiency of 90% in the electron range expected from τ-decay and a rejection of 70 against charged pions. These figures are obtained by using an analysis similar to the one of NA31. The performances increase with the number of radiators considered. The rejection reaches 1000 with 6 radiators.

Two types of TRD are being considered at present:

- Two layers of 3 m long vertical straw-tubes with a diameter of 1 cm and 25 μm thick walls of graphite-coated mylar. These tubes use pure Xe at atmospheric pressure and are mounted on a frame which keeps them straight by applying a suitable pull at one end of the straw-tube. The total number of tubes in the entire detector is 12000. A prototype system consisting of several 2.5 m long straw-tubes has been built and successfully tested at CERN by an Orsay group (7).
- If the straw-tubes option shows difficulties, we would adopt a multiwire proportional chamber similar to the design of the NA31 experiment (6). The polypropylene foils of the radiator are immersed in a CO_2 volume at atmospheric pressure and the chamber is filled with a mixture of $Xe/Ne/CH_4$ at atmospheric pressure in the ratio 30/55/15, which has the same density as CO_2. This choice equalises the hydrostatic pressure on both sides of the thin chamber entrance window and thus ensures its flatness over the entire area of 3*3 m^2. The chamber has 250 vertical sense wires with a spacing of 1.2 cm, located at a distance of 2.5 cm from two graphite-coated 75 μm thick mylar foils which act at the same time as cathode planes and windows. Using this design the total number of sense wires in the entire detector is 5000.

In both TRD designs the electronics consist of simple 6-bit ADC's to record the

individual pulse heights from the wires. High-energy electrons are identified by the larger pulse height associated with the transition radiation X-rays.

3.2.3 Drift chambers

A drift chamber is located just behind each TRD to measure charged particle momenta. The proposed design is illustrated in Fig. 4. Each chamber consists of two independent gaps with the horizontal (parallel to B) sense wires shifted by half the drift cell size to remove the left-right ambiguity. In the drift region the electric field has two components, one (E_D) parallel to the drift direction, and the other (E_C), perpendicular to both the drift direction and B, needed to compensate the effect of the magnetic field so that the electrons drift along the vertical direction. This electric field is generated by suitable field-shaping wires. For a typical drift velocity of 5×10^4 m/s, E_C is proportional to B and is 350 V/cm for B=0.7 T. This design was successfully run in the past (8).

The chamber resolution along the drift direction is $\sigma = 200$ μm. The particle coordinate along the wire is measured by charge division with a resolution $\sigma = 3$ cm (1% of the wire length). Each chamber contains 120 sense wires, totalling 2400 sense wires for the entire detector.

3.2.4 Electromagnetic calorimeter

An electromagnetic calorimeter is located at the end of the target volume covering the whole surface area of the magnet. It has two purposes:
- it measures the candidate electron energy in order to check the consistency between energy and momentum
- it measures photon energies and angles in order to add their energies in the measurement of the p_t of the event.

Monte-Carlo simulations show that the absence of hadronic calorimetry does not introduce additional backgrounds in the search for a ν_τ signal.

We intend to use a lead-scintillator calorimeter consisting of planes of 1 cm thick scintillator tiles alternating with planes of 3 mm thick lead (see Fig. 5). Each tile is read by a WLS fiber embedded in a groove machined in the tile surface. The WLS fiber emerges from the scintillator surface near a tile boundary and is fused to a clear fiber which is then routed along the scintillator surface to the edge of the calorimeter. The tiles are 10*10 cm^2 in area. The fibers reading tiles which are directly behind each other are grouped together and go to the same photomultiplier thus yielding a tower geometry. The WLS fibers in successive tiles are oriented at 90° to each other to improve the uniformity of the response. The calorimeter will consist of 30 scintillator pieces alternating with 30 lead planes for a total of 22 X_0 .It will have 900 channels. The expected energy resolution is $\sigma = 0.15/\sqrt{E}$ (E in GeV).

Another possibility, considered as a back-up solution, is to use a calorimeter of the UA2 type read-out by wave-shifting plates on the cell side.

3.2.5 Muon filter

The end return yoke of the magnet serves as part of the muon filter which will be complemented by a second block of 1 m thick iron or 2 m concrete. The UA1 chambers of dimensions 4*3.5 m^2 are available for the muon detection.

3.2.6 Trigger

A hodoscope of scintillators put in front of the target vetoes on incoming particles. It covers the full entrance area. Two hodoscopes, one at the end of the fiducial volume and one in front of the calorimeter are used for triggering purposes. If the rate were too high one could require a signal in the calorimeter to trigger on electrons, and a signal behind the iron to trigger on muons.

3.3 Electron identification and measurement

The set-up allows several independent signatures of electrons. If an electron is produced in radiator set n, one can follow the track in all the successive modules. Already the information of sets $n+1$ and $n+2$ gives an efficiency of 99%. When the track exits from the target it is absorbed in the electromagnetic calorimeter. By checking the consistency between the measured momentum and the deposited energy, one identifies again electrons with a high confidence level. In typical collider experiments, this method gives a rejection of 10^3 against other particles. The electron starts showering before it leaves the target, the total length representing 45% of a radiation length. Electrons lose energy by bremsstrahlung. In bubble chambers this loss is divided in soft and hard radiation. A hard brem is defined to be an energy loss visible as a kink in the electron track. Soft brems give a smooth energy loss. In our case hard radiation can be accounted for by adding any radiation emitted tangent to the electron direction. In all cases the true momentum and direction are measured over the first part of the trajectory where the energy loss is limited to a few per cent. On average 40% of the electron energy is lost per radiation length. Still the charged track which reaches the calorimeter must pass the consistency test between the momentum measured in the last gaps and the energy.

Combining the transition radiation information and the p/E criterion gives a very powerful signature for electrons with a rejection against pions reaching 10^6. It is interesting to notice that electrons also produce synchrotron radiation at approximately the same wave length as TRD. This should enhance the signal and improve the signature of electrons in the set-up.

4. ANALYSIS

4.1 Kinematical cuts

We have defined a series of cuts to search for the appearance of the ν_τ, taking advantage of the kinematic differences between CC ν_τ and CC ν_μ or ν_e interactions. To do this, neutrino interactions have been generated using the Lund Monte-Carlo program. Neutrons and K_L are assumed to be undetected. Charged tracks are followed if they have more than 0.5 GeV/c momentum. Photons from decays are assumed to be reconstructed in the angular acceptance of the electromagnetic calorimeter if they have an energy of more than 500 MeV.

The momentum resolution for charged tracks takes into account multiple scattering and chamber resolution. A magnetic field of 4 kG was chosen. Fig. 6 shows the resolution for charged tracks produced in the first part of the target, in the middle part, and the last part of the fiducial volume. The energy resolution of the calorimeter is taken equal to $15\%/\sqrt{E}$ and its granularity is 10*10 cm^2.

We limit the study to events having an electron. They come from either:

$$\nu_e + N \rightarrow e^- + X$$

with the spectrum of Fig. 1 or

$$\nu_\tau + N \rightarrow \tau^- + X$$

followed by the decay : $\tau^- \rightarrow e^- \nu \bar{\nu}$. The spectrum used here is the one of ν_μ.

Fig. 7 shows the electron spectra, at production coming from τ decays, CC ν_e interactions and Dalitz π^0 decays respectively. Fig. 8 shows the production angles with respect to the neutrino beam for the case of electrons and charged hadrons.

In τ decays, two neutrinos are produced. This gives a large missing momentum p_t in the plane transverse to the incident neutrino direction. The distribution of the missing p_t is shown in Fig. 9 for ν_τ and ν_e separating the various contributions to the missing p_t.

The discrimination between ν_τ and ν_e CC events is particularly clear when considering the angle φ_1 between the missing p_t and the transverse momentum of the hadronic system, and the angle φ_2 between the lepton and the hadrons. These parameters are defined in Fig. 10. Figure 11 shows the respective scattered plots of φ_1 versus φ_2 for the cases of ν_τ and ν_e separately.

The selection is done with the following conditions:
- the event has a combination (φ_1, φ_2) as shown in the figure by the dashed line
- the electron reaches the calorimeter
- its energy is greater than 1.5 GeV
- its transverse momentum with respect to the measured hadronic system is greater than 300 MeV/c
- the smallest invariant mass it reconstructs with a photon is greater than 240 MeV
- the total visible energy is less than 50 GeV

Table 1 shows the effect of these cuts on ν_τ events giving an electron, ν_e events and NC events with a Dalitz decay.

The efficiencies to retain ν_τ and ν_e events become respectively 21% and 0.045%.

This analysis is only based on the electronic decay of the τ. Other decay modes such as the 3 pions channel or the ρ^- channel decaying into $\pi^- \pi^0$ require further studies.

4.2 Background

There are various sources of background, some coming from real electrons and others from fake electrons. Real electrons are produced in CC ν_e interactions but also in CC ν_μ interactions giving charm, and in CC or NC ν_μ interactions with Dalitz decays of π^0. These various sources are included in the Monte Carlo.

The background from ν_e interactions comes from events remaining after the cuts defined previously. This can be precisely known by applying the same cuts to the much more abundant ν_μ sample which is kinematically identical. With 770000 ν_μ events, one expects 350 remaining events. The small contribution of ν_τ interactions in the muon sample is negligible. The number of ν_e events passing the cuts is then known to 5% and can be safely subtracted.

We expect 5400 CC ν_μ events giving a charm meson decaying into a positron. These are the so-called μe events. With a 10% probability of missing the muon there remain 540 events with a positron alone. A signal of true electron can only come from $\bar{\nu}_\mu$'s which are present in the beam at the reduced level of 5%. Furthermore the charm cross- section for $\bar{\nu}_\mu$ is four times smaller than that of ν_μ. These few events are included in the Monte-Carlo and are rejected by the kinematical cuts. Neutral currents pair-produce charm at a negligible level.

True electrons can also arise from Dalitz decays of π^0 and η or charged Ke_3 decays in NC interactions. The asymmetric Dalitz are dominant. For an expected statistics of 260000 events the Monte Carlo program gives a total of 5300 π^0 or η with a Dalitz pair. Among these only 140 have an electron of more than 1.5 GeV hitting the calorimeter and no visible positron. The cut for the positron is chosen at 100 MeV/c. Further cuts on the electron transverse momentum with respect to the hadron jet and the invariant mass formed by the electron and a photon are also applied. They leave a total of 2.1 events. It is to be noted that the Dalitz pair production is measured in the experiment, and the background from asymmetric pairs can be estimated by the sample of positrons equally produced, and by the corresponding signal in CC events.

Another background comes from fake electrons. They will happen in neutral current events, since we require no muon detected and a sizable missing p_t . They arise from charged pions misidentified in the transition radiation detector, and subsequently superimposed with neutral pions in the calorimeter. This background is extremely small and again precisely known by counting events having a muon and a misidentified electron in the hadronic jet. Furthermore it is charge symmetric. These events, if any, are efficiently removed by the kinematical cuts.

Photons produced in the interaction can convert asymmetrically in a region of confusion close to the vertex or Compton scatter on electrons. Due to the very low density target, this is estimated to be less than the Dalitz background.

5. ACHIEVABLE LIMITS

5.1 Statistics

The full statistics considered here is 770000 events. Among these 700000 have a well reconstructed muon. The relative flux of ν_e is 0.7%. This is integrated over the whole spectrum which is harder for ν_e than for ν_μ. In the analysis, only the low energy part of the spectrum is kept. The corresponding number of electron events is around 7700. In this experiment, the relative flux of ν_e is directly calculated since events with a true electron are recorded and their energy measured. The problematic estimation of the beam contamination, which is the main limitation in oscillation searches, is avoided.

With the entire set of kinematical cuts, one keeps 21% of the ν_τ events and only 0.045% of the ν_e events and 0.04% of the Dalitz pairs. These backgrounds are known precisely as explained earlier by the analysis of the ν_μ events and the comparison of negative and positive tracks.

If no signal is detected, a limit at 2.3 events can be set at 90% confidence level. With our set of cuts, the reduction factor for the ν_τ cross-section due to the τ mass is 0.6. With this correction, the branching ratio of $\tau \rightarrow$ e (17.8%) and the efficiency to retain ν_τ events (0.21), one finds a maximum signal of 102 events attributable to ν_τ. With the background estimated at 5.6 events, this number becomes 234. This is to be compared to the full sample of 770000 events.

5.2 Detection of oscillations

Assuming the only electronic channel of τ-decays as discussed here, the sensitivity lies between 1.3×10^{-4} and 3.0×10^{-4} at 90% CL for the maximum fraction of ν_τ measurable in the ν_μ beam. The limit on $\sin^2 2\,\theta$, for large values of δm^2 becomes 2.6×10^{-4} to 6×10^{-4}. The cuts may still be improved, and other possible τ decay channels could be used to strengthen further the search.

The present limit translates into an exclusion region in the $\sin^2 2\theta$, δm^2 plot. Assuming a distance of 940 m to the production target and an average energy of 27 GeV, the result is presented in Fig. 12. It improves by more than one order of magnitude the previous best limit (3). In particular it covers the region of large ν_τ masses (>10 eV) and small mixings (10^{-3}) advocated in Ref. 1.

The limit obtained for the oscillation $\nu_e \rightarrow \nu_\tau$ is also represented in Fig. 12. It gives $\sin^2 2\theta < 3.6 \times 10^{-2}$ for large masses. This is obtained from the ν_e contamination of the beam. In terms of the Kobayashi-Maskawa matrix element, this translates into a limit $|U_{e\tau}|^2 < 0.9 \times 10^{-2}$ smaller than the claim of (2).

6. MEASUREMENT OF OTHER PHYSICAL PROCESSES

The experiment is not limited to the search of oscillations.

6.1 Standard physics

The detector emphasizes a very good electron identification and measurement.This allows an improved study of charm production by neutrinos in the channel where the charm quark decays into an electron. Furthermore the signal of same sign dilepton events is still unresolved with some experiments seeing it an others not. The experiment can improve by an order of magnitude the exploration of the channel μ^-e^-.

6.2 Investigation of e.m. properties of neutrinos

The detector is ideally suited to see electrons and photons down to very low thresholds. A candidate electron can be recognized if it traverses one module. A minimum energy of 100 MeV/c is detectable. This limit is imposed by the magnetic field and not by dE/dx. The signature for photons is even cleaner giving two tracks radiating in the modules. A trigger based on the TRD chambers has to be developed for this purpose.

This property of the detector can be exploited to search for processes of the type:

$$\nu + e \rightarrow \nu + e \qquad \nu + \gamma \rightarrow \nu + \gamma \qquad \nu + e \rightarrow \nu + e + \gamma$$

The scattering off photons has still to be calculated theoretically. For the scattering off electrons, the electroweak level predicts 180 events. Very precise energy and direction measurements of the outgoing electron are obtained in the proposed set-up.

More interestingly the same channel offers a way to push the present limit on the magnetic moment. The cross-section for a magnetic moment μ (expressed in unit of Bohr magneton) to give an electron above 100 MeV/c is: $\sigma = 10^{-24}\ \mu^2$ (10). These electrons are peaking at low energy, contrary to the ones produced in the electroweak process. The beam contains a small fraction of ν_τ coming from D_S decays. The relative flux can be evaluated at 10^{-6}. This is negligibly small for the oscillation search but would result in a signal of 300 events if the magnetic moment were as high as its present limit of 8.2 $10^{-6}\ \mu_B$ (11). If the oscillation is found at the level of 10^{-4}, suggested by the existence of the 17 keV neutrino state, the same magnetic moment would give 30000 events showing an isolated electron, clearly a conspicuous signal! In that case one could set a limit down to $\sim 10^{-7}\ \mu_B$.

Based on the see-saw mechanism, one can argue that such a ν_τ magnetic moment is equivalent to a ν_e magnetic moment of $10^{-14}\ \mu_B$, well below the value necessary to explain the solar neutrino puzzle.

7. COST ESTIMATES

Moving of the UA1 magnet	
Estimation by CERN engineers, including an existing platform	250 kSF
Construction of the polypropylene radiators	
Extrapolation of the NA31 figure for material and construction	250 kSF
Xenon chambers	
- construction : 20 planes of 600 tubes 3 m long	400 kSF
- electronics (preamp, 6-bit ADC, memory)	720 kSF
Drift chambers	
- construction: Estimation from STIPE Saclay for 20 planes of 3*3 m^2	2500 kSF
- electronics: 2400 channels	840 kSF
Electromagnetic calorimeter	1300 kSF
- electronics (2 samplings)	350 kSF
Scintillator hodoscopes	
Veto and trigger, hodoscopes	150 kSF
Muon filter	
Installation of existing UA1 chambers	50 kSF
Data acquisition	1000 kSF
Mechanics	500 kSF
Gas System	500 kSF
Xe gas	200 kSF
TOTAL:	9 MSF

8. CONCLUSION

Massive neutrinos come in theories which go beyond the standard electroweak theory so succesfully tested in many precision measurements. As a consequence, the discovery of oscillations or of anomalous electromagnetic properties of the neutrinos, would be a first sign of what happens beyond the energy scale of 100 GeV.

Arguments from astrophysics support a ν_τ mass as high as a few 10 eV. The solar neutrino puzzle can be explained by a large magnetic moment of the neutrino. The present experiment tries to give some inputs into those two fundamental questions.

Using only kinematical criteria implemented in a set-up which does not require the development of any new technique, the sensitivity to oscillations in the channel $\nu_\mu \rightarrow \nu_\tau$ can be pushed to at least one order of magnitude better than previous searches in the region of small mixing angles. If oscillations are not found at this level, it can be argued that light neutrinos are probably not responsible for the missing mass of the Universe. This search also tests the existence of a 17 keV mixing with the ν_e.

In parallel the experiment measures with accuracy several processes which require an excellent electron identification. This program is fulfilled in an experiment which im-

plements a new way of looking at neutrino interactions using a transparent target. The required techniques are all well-known and do not necessitate difficult developments.

REFERENCES

[1] H. Harari Phys.Lett. **B216** 413 (1989).

[2] J.J. Simpson and A. Hime Phys. Rev. **D39** 1825 (1989).
A. Hime and J.J. Simpson Phys. Rev. **D39** 1937 (1989).
A. Hime and N.A. Jelly 'New evidence for a 17 keV neutrino' Submitted to Physics Letters B.

[3] N. Ushida et al. Phys. Rev. Lett. **57** 2897 (1986).

[4] Proposal Charm2 Collaboration CERN-SPSC/90-42.
K. Kodama et al. Draft Proposal. Fermilab P803.

[5] C. Albright et al. Phys. Lett. **84B** 123 (1979).
M. Poppe et al. Phys. Lett. **100B** 84 (1981).
H. Talebzadeh et al. CERN/EP 87-47.

[6] A. Vacchi NIM **A252** 498 (1986).
G.D. Barr et al. CERN-EP/90-62
B. Dolgoshein NIM **A252** 137 (1986).

[7] R. Cizeron et al. 'Results from beam tests of a 2.4 m straw chamber'. Submitted to NIM.

[8] L.Camilleri et al. NIM 156, 275 (1978).

[9] M.G. Albrow et al. NIM **A256** 23 (1987).
G.R. Snow 'A novel triggering system for the UA6 e.m. calorimeter' Int. Conf. on calorimetry. Fermilab 29 oct.-1 nov. 1990.

[10] A.V. Kyuldjiev Nucl.Phys. **B243** 387 (1984).

[11] N.G. Deshpande and K.V.L.Sharma OITS 448.

FIGURE CAPTIONS

Figure 1 Energy spectrum of the SPS wide band neutrino beam.

Figure 2 Overall view of the detector. Not shown is a hodoscope at the end of the fiducial volume.

Figure 3 Structure of the target showing the polypropylene radiators together with the Xe tubes and the drift chambers.

Figure 4 Design of the drift chamber.

Figure 5 The electromagnetic calorimeter.

Figure 6 Momentum resolution obtained for charged tracks in three regions of the target: first part, middle part and end part.

Figure 7 Electron spectra for the cases of ν_e interactions, CC ν_τ interactions and Dalitz background.

Figure 8 Production angles for electrons and charged hadrons with respect to the beam.

Figure 9 Histograms of the missing p_t showing the various contributions, in the case of ν_τ (full line) and ν_e (dashed line).

Figure 10 Definition of the kinematical parameters.

Figure 11 Scatter plots of the angle in the transverse plane between the missing p_T and the hadrons, versus the angle between the electron and the hadron jet. The dashed curve shows the retained region.

Figure 11a refers to ν_τ events.

Figure 11b refers to ν_e events.

Figure 12 Exclusion regions in the oscillation plot.

cuts	$\nu_\tau \rightarrow \tau \rightarrow e^-$	$\nu_e \rightarrow e^-$	N.C. with Dalitz
	100	100	100
$E_{e^-} > 500MeV$	95.3	98.0	38.0
$E_{e^+} < 100MeV$	90.3	94.3	2.6
e^- in the calorimeter	79.0	92.3	1.43
ϕ scatter plot cut	35.0	0.32	1.37
$E_{visible} < 50GeV$	29.2	0.13	1.25
$E_{e^-} > 1.5GeV$	26.2	0.13	0.48
$m(e^-\gamma) > 240MeV$	22.0	.064	.081
$P_T^{e^-/hadrons} > 300MeV$	20.8	.045	.035

Table 1: Reduction of the simulated samples through the successive kinematical cuts.

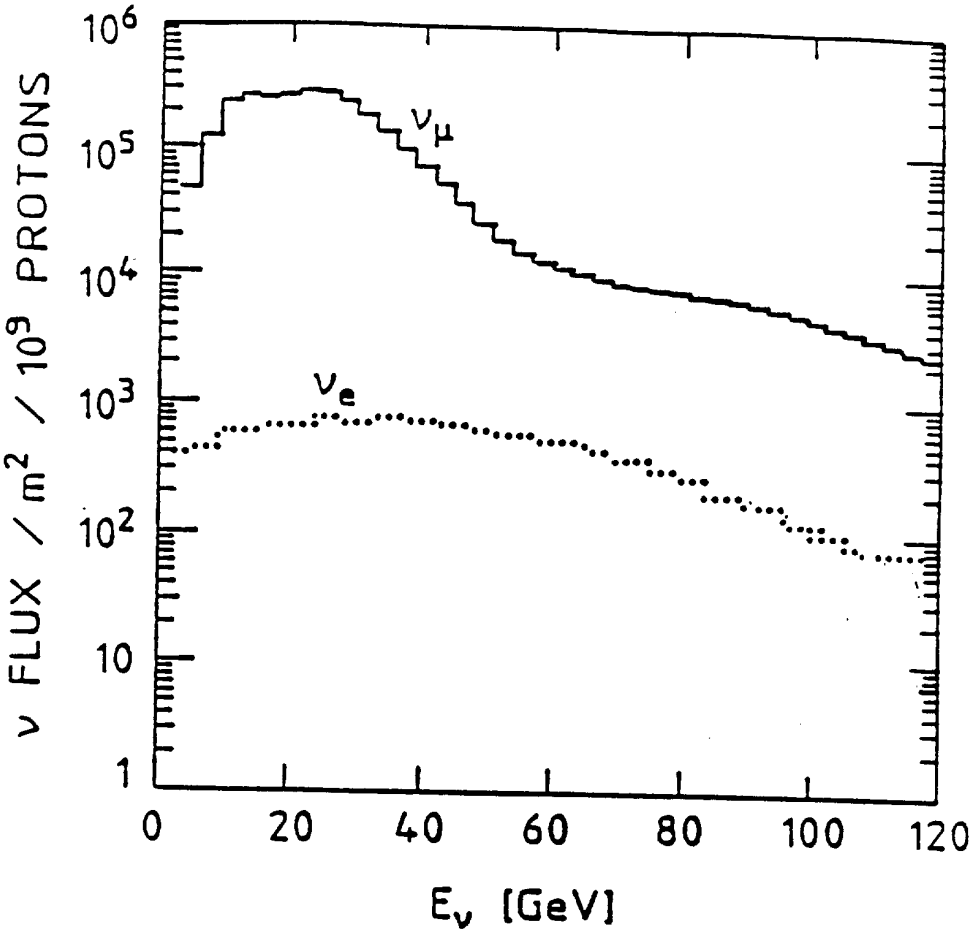
10^6
10^5
10^4
10^3
10^2
10
1
ν FLUX / m^2 / 10^9 PROTONS
ν_μ
ν_e
0
20
40
60
80
100
120
E_ν [GeV]

Fig. 1

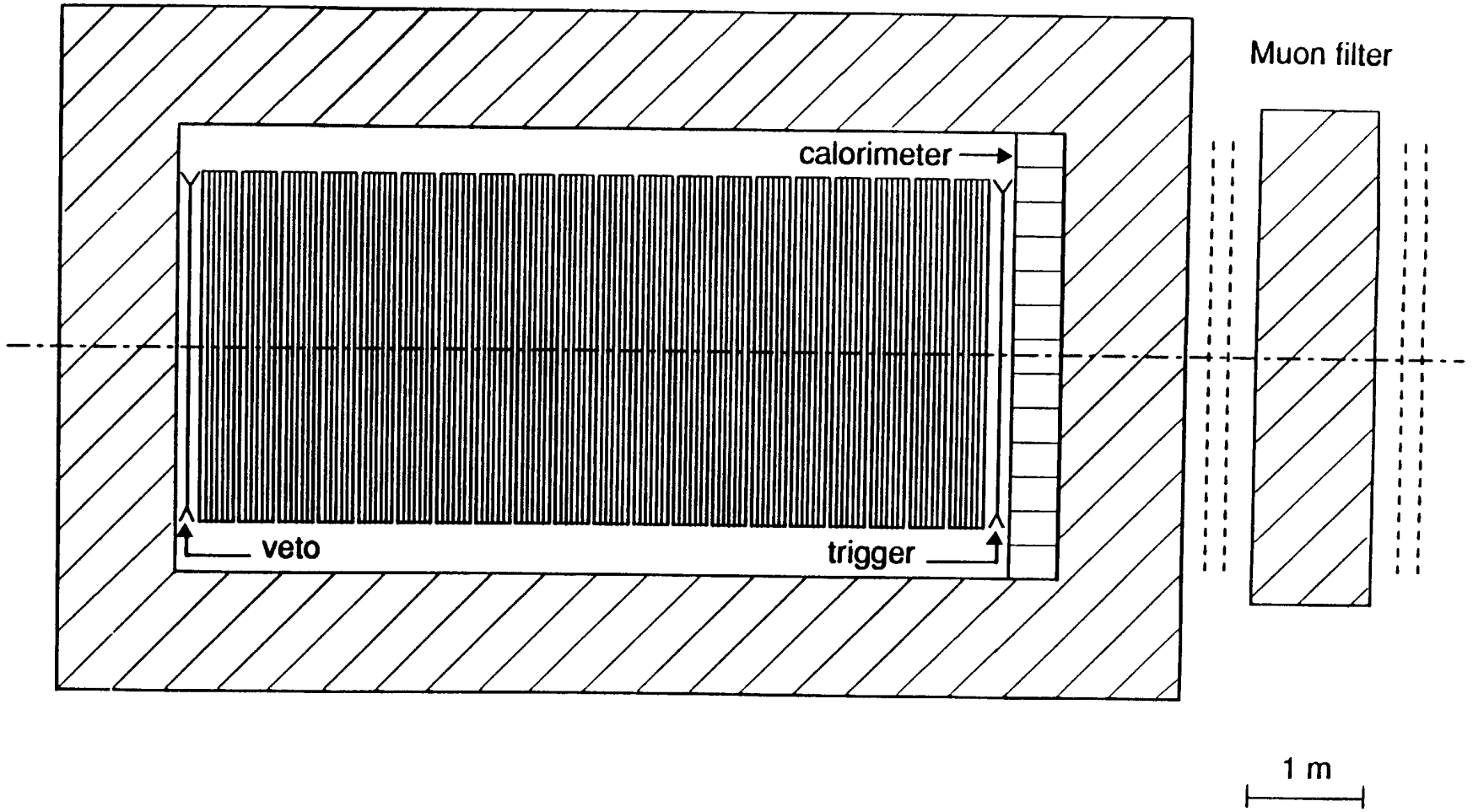

Fig. 2

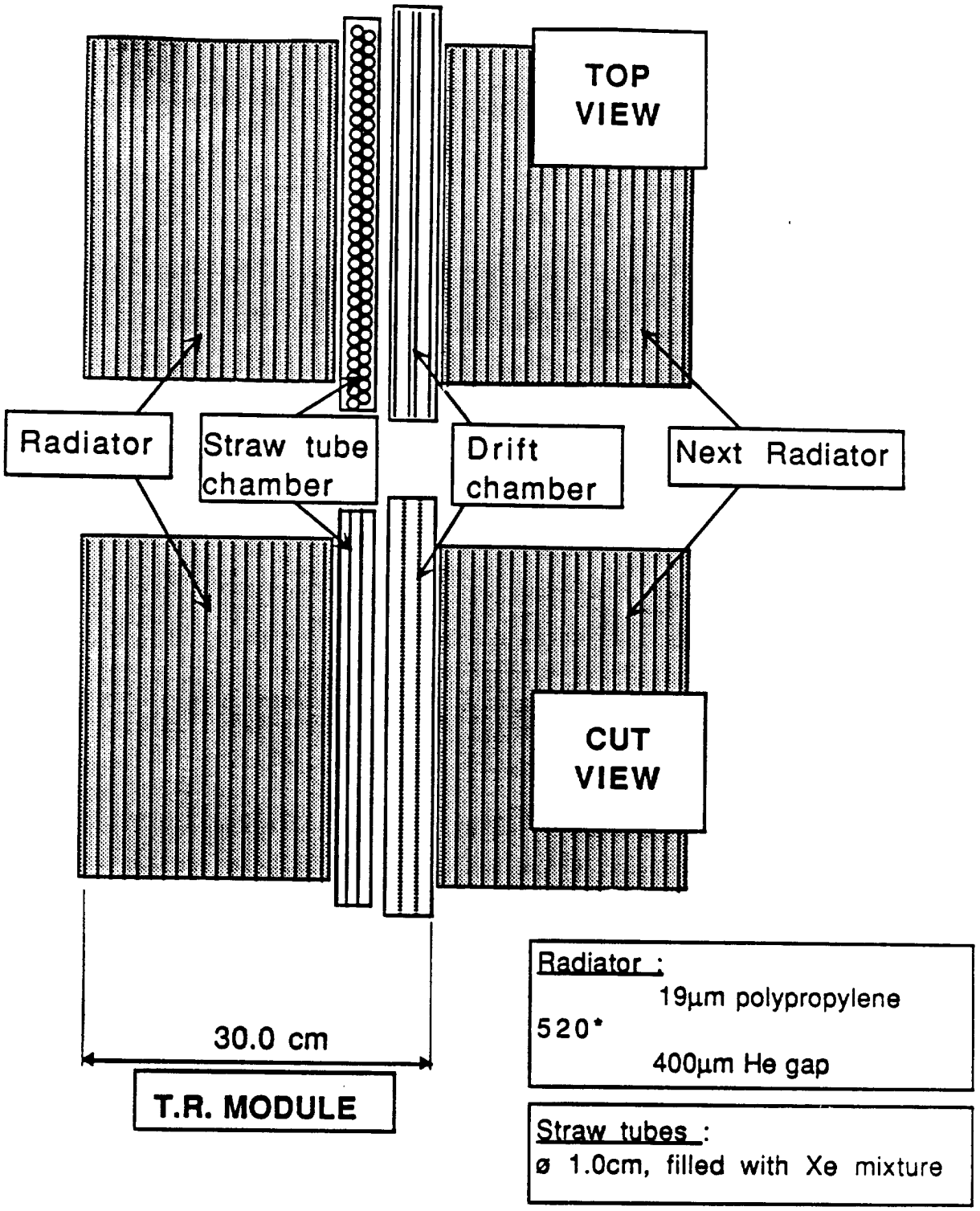
TRANSITION RADIATION DETECTOR
TOP VIEW
Radiator
Straw tube chamber
Drift chamber
Next Radiator
CUT VIEW
30.0 cm
T.R. MODULE
Radiator :
19μm polypropylene
520*
400μm He gap
Straw tubes :
ø 1.0cm, filled with Xe mixture

Fig. 3

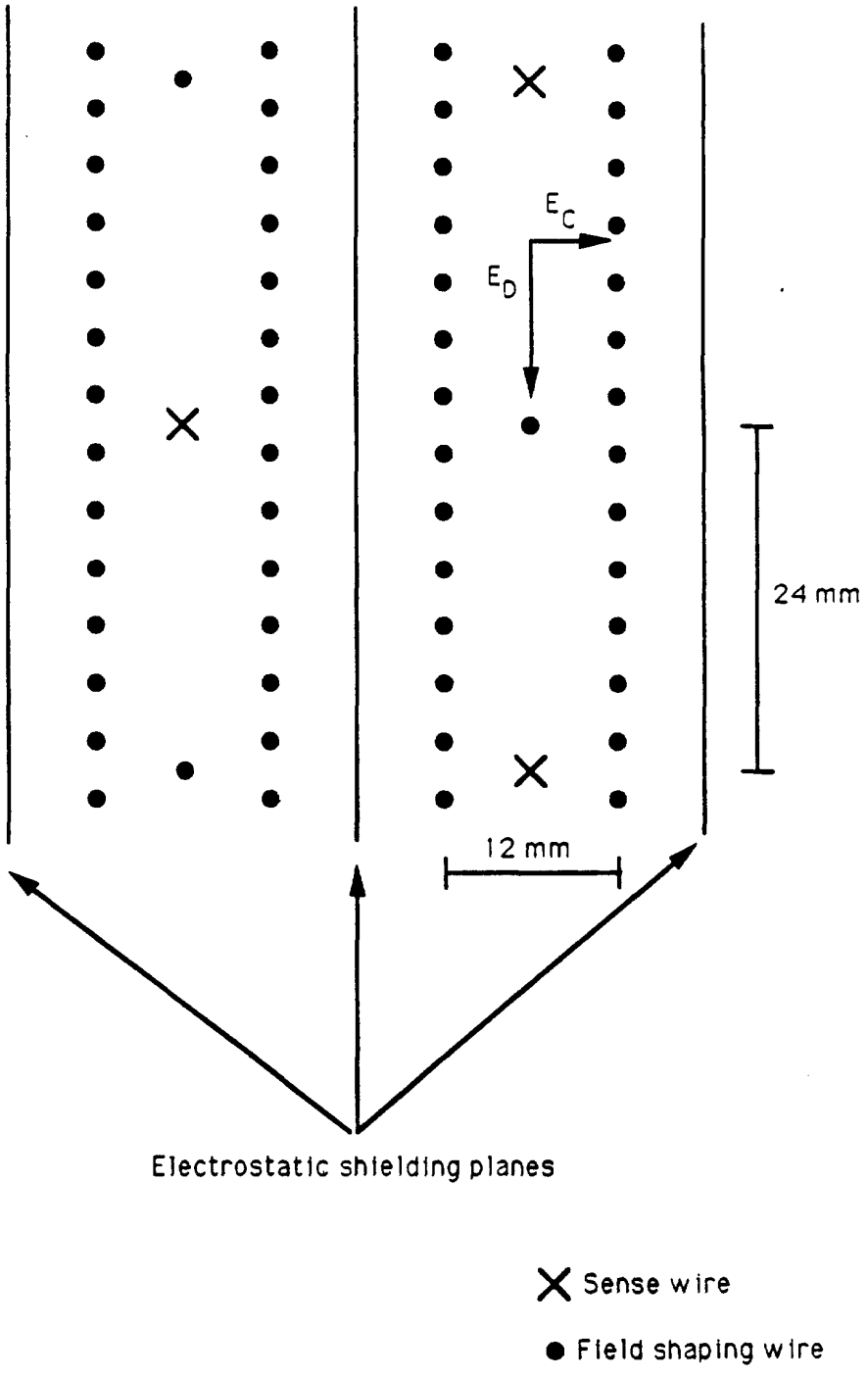
E_C
E_D
24 mm
12 mm
Electrostatic shielding planes
Sense wire
Field shaping wire

Fig. 4

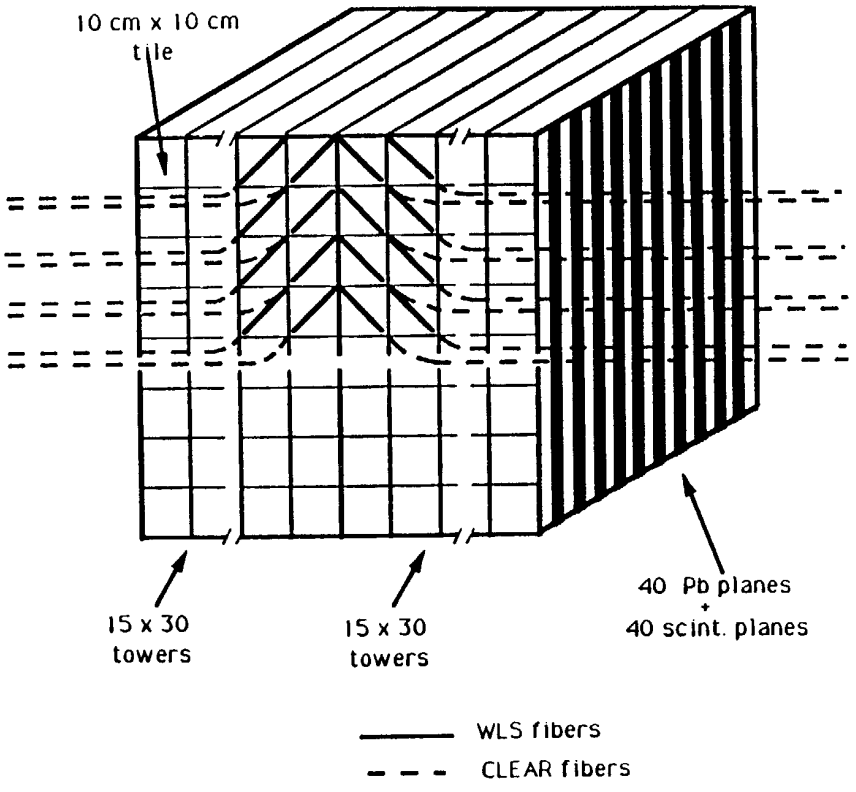
10 cm x 10 cm
tile
15 x 30
towers
15 x 30
towers
40 Pb planes
+
40 scint. planes
WLS fibers
CLEAR fibers

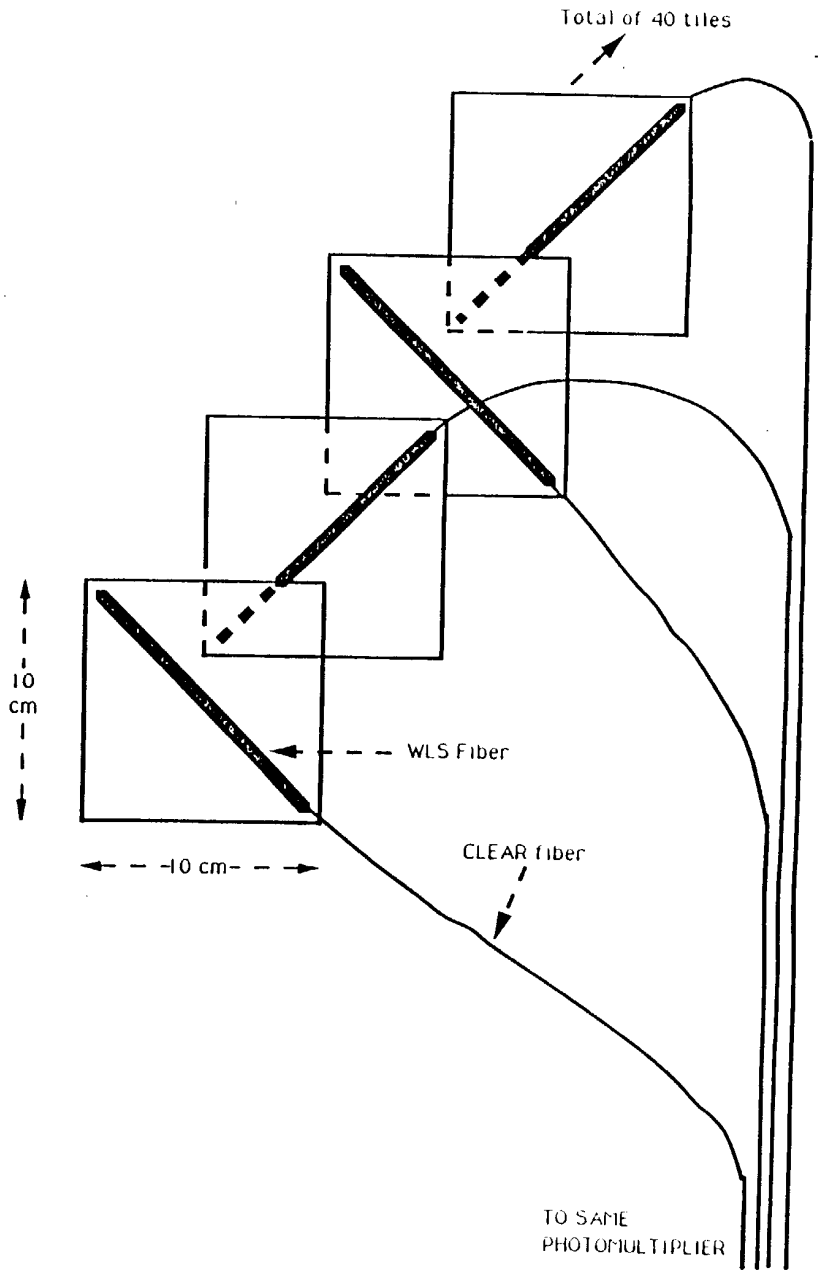
Total of 40 tiles
10
cm
WLS Fiber
10 cm
CLEAR fiber
TO SAME
PHOTOMULTIPLIER

Fig. 5

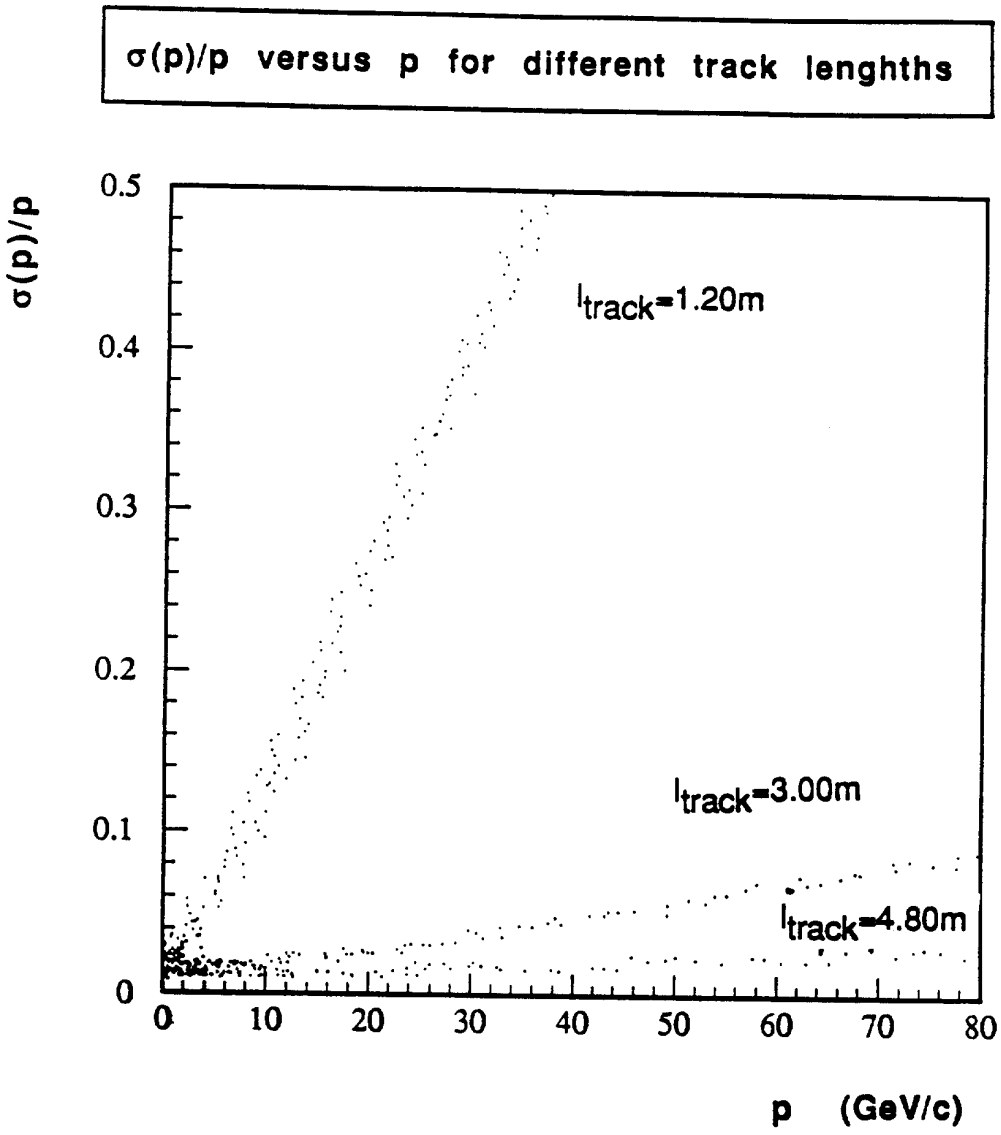
σ(p)/p versus p for different track lenghths
σ(p)/p
0.5
0.4
0.3
0.2
0.1
0
0
10
20
30
40
50
60
70
80
p (GeV/c)
l_track=1.20m
l_track=3.00m
l_track=4.80m

Fig. 6

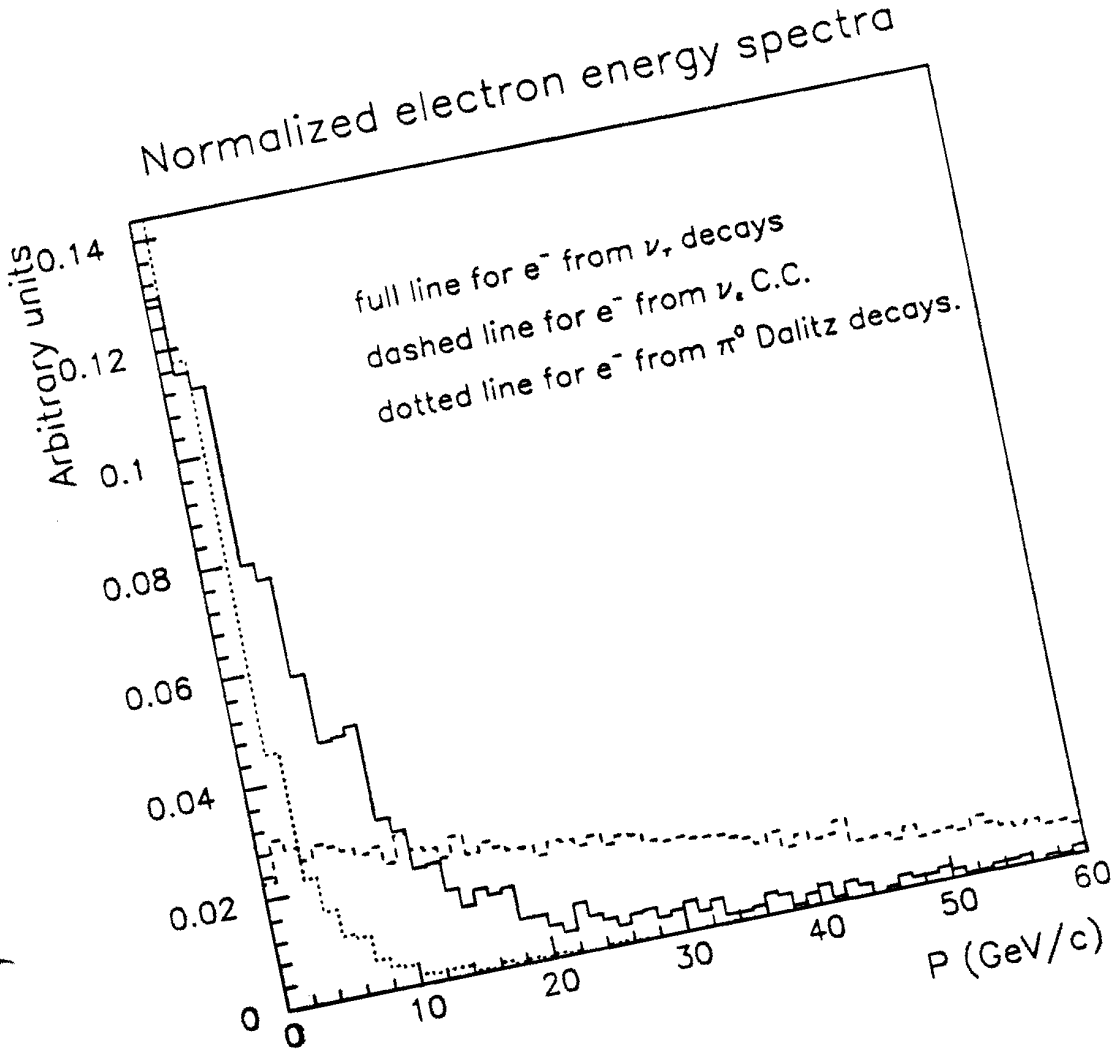
Normalized electron energy spectra
full line for e⁻ from ν_τ decays
dashed line for e⁻ from ν_e C.C.
dotted line for e⁻ from π^0 Dalitz decays.
Arbitrary units
0.14
0.12
0.1
0.08
0.06
0.04
0.02
0
0
10
20
30
40
50
60
P (GeV/c)

Fig. 7

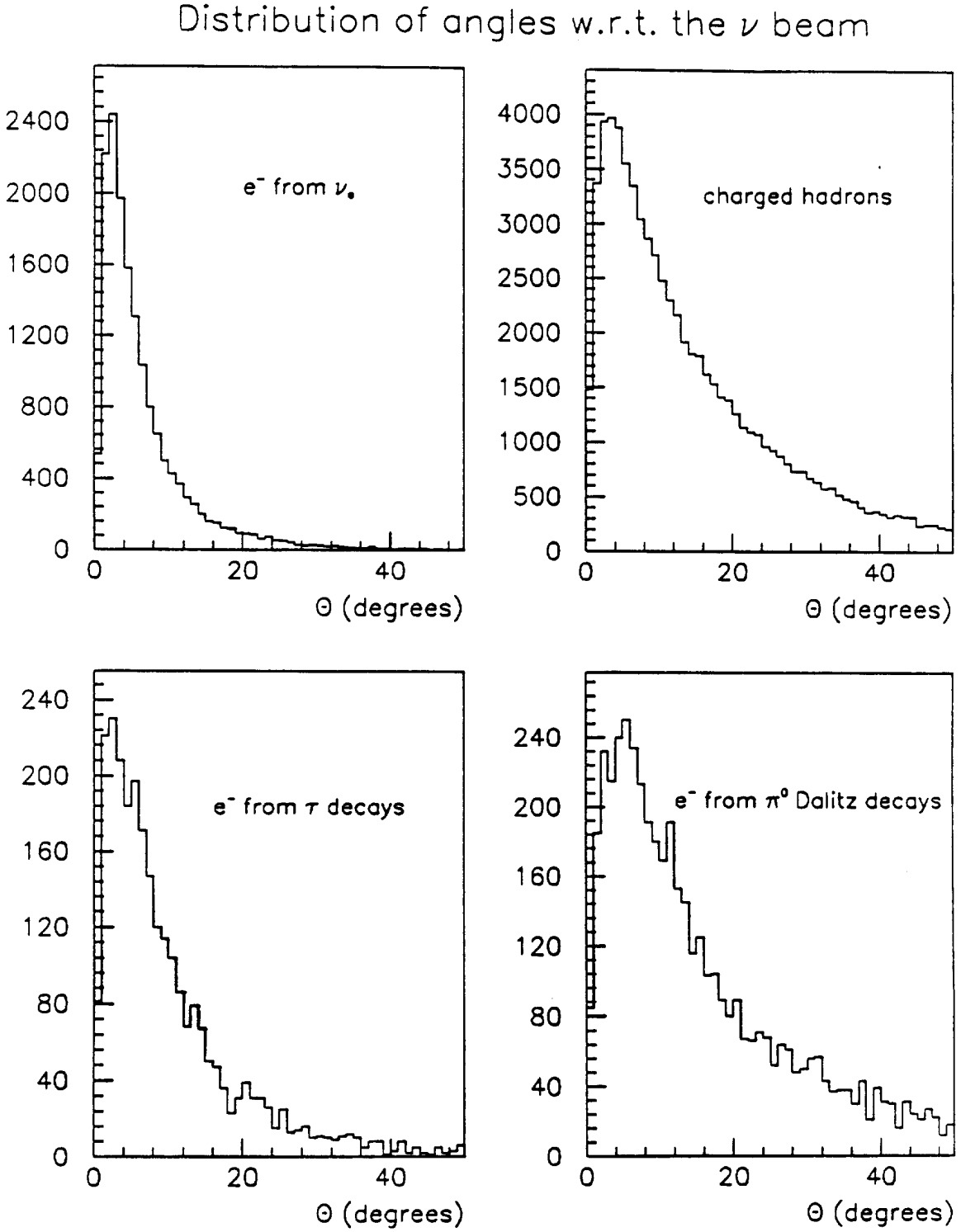
Distribution of angles w.r.t. the ν beam
e⁻ from ν_e
charged hadrons
e⁻ from τ decays
e⁻ from π⁰ Dalitz decays
Θ (degrees)
Θ (degrees)
Θ (degrees)
Θ (degrees)

Fig. 8

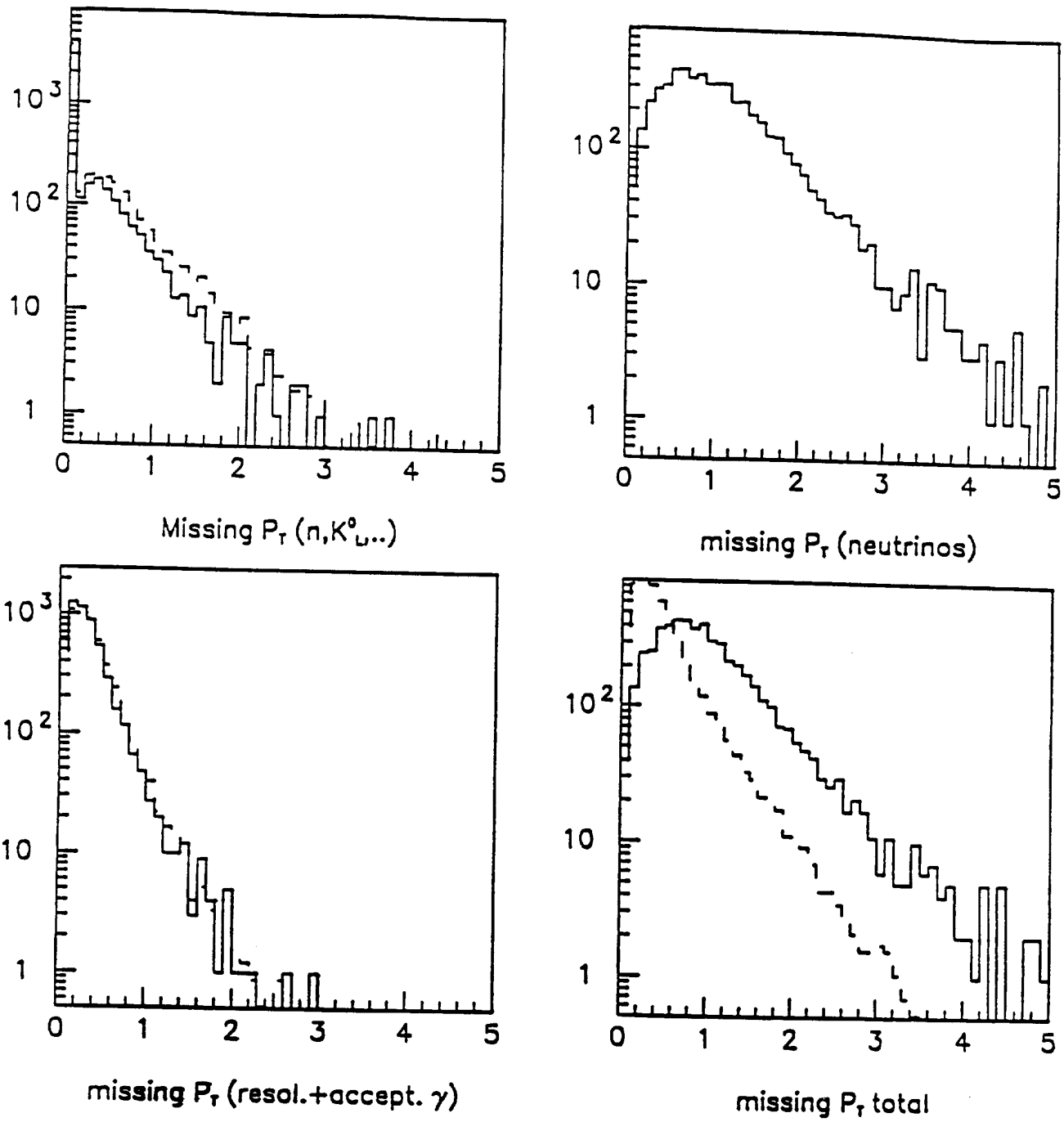
Missing P_T (n,K^0_L..)
missing P_T (neutrinos)
missing P_T (resol.+accept. γ)
missing P_T total

Fig. 9

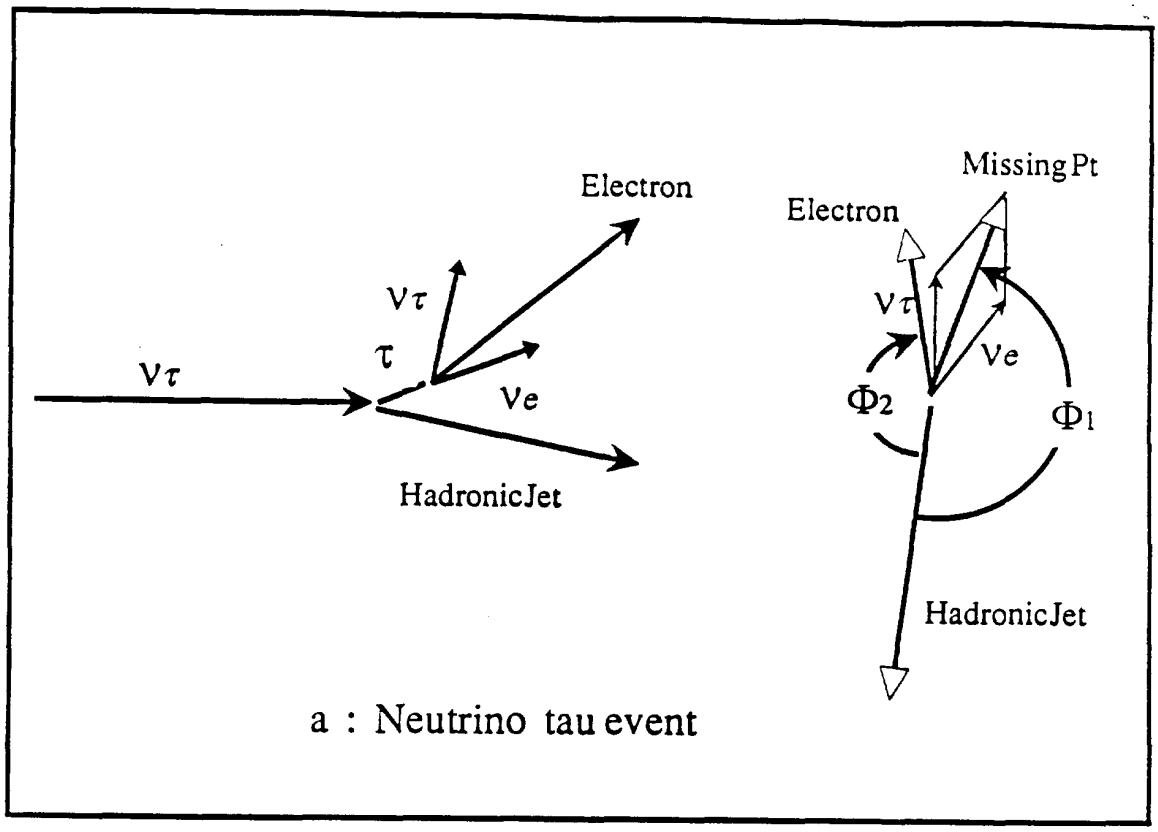

a : Neutrino tau event

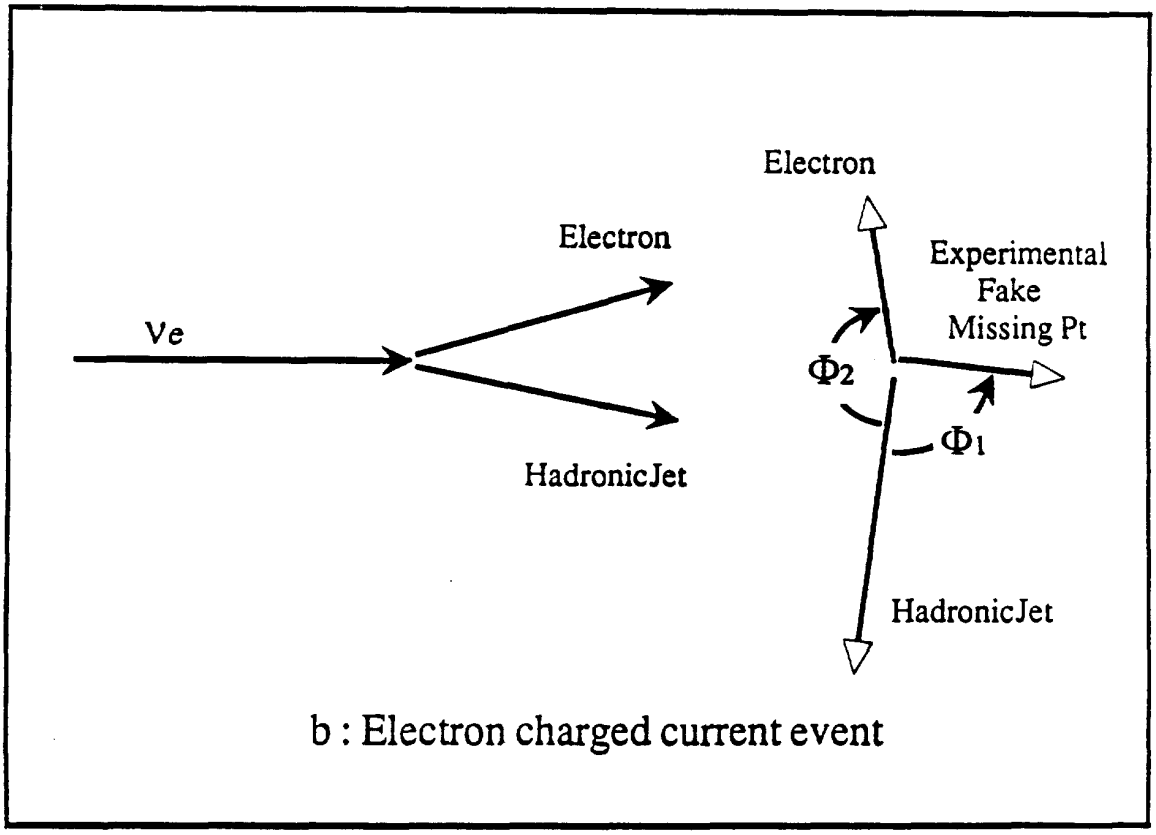

b : Electron charged current event

Fig. 10

ν_τ ν_e

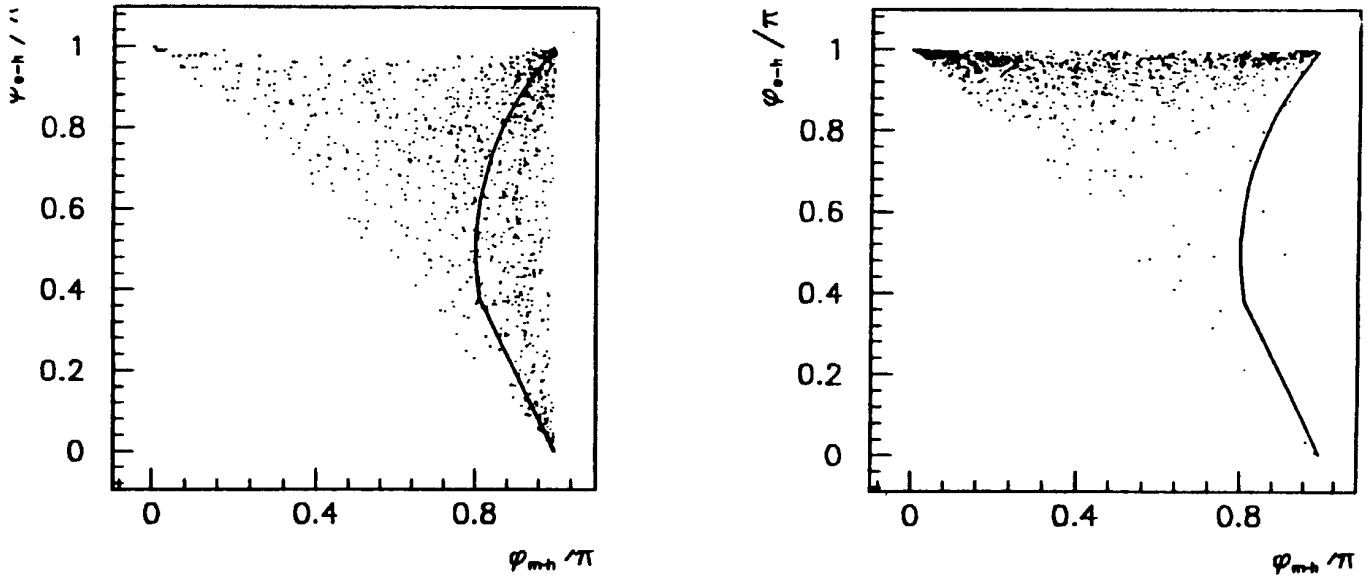

$\varphi_{e\text{-}h}$ versus $\varphi_{m\text{-}h}$

Fig. 11

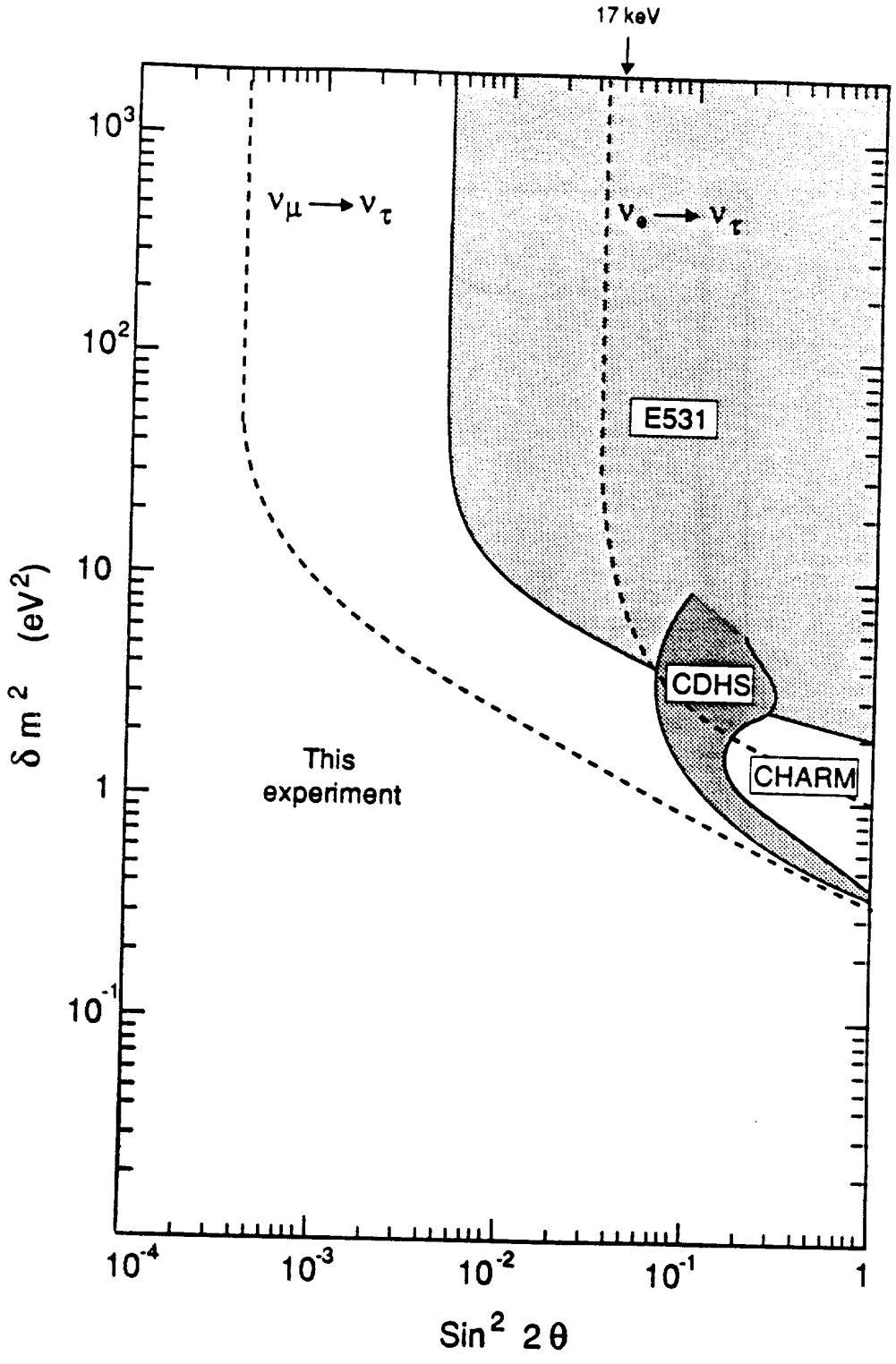
17 keV
$\nu_\mu \rightarrow \nu_\tau$
$\nu_e \rightarrow \nu_\tau$
E531
CDHS
CHARM
This
experiment
δm^2 (eV^2)
10^3
10^2
10
1
10^{-1}
10^{-4}
10^{-3}
10^{-2}
10^{-1}
1
$\sin^2 2\theta$

Fig. 12